CHAPTER III

n-OCTANE AROMATIZATION ON A Pt/KL CATALYST PREPARED BY VAPOR-PHASE IMPREGNATION

Siriporn Jongpatiwut, Paneeya Sackamduang,
Thirasak Rirksomboon, and Somchai Osuwan

The Petroleum and Petrochemical College,
Chulalongkorn University, Bangkok, Thailand

and

Daniel E. Resasco*

School of Chemical Engineering and Materials Science,
The University of Oklahoma, Norman, OK 73019

Submitted to *Journal of Catalysis*
April, 2002

Keywords: *n-octane aromatization, Pt/KL, Pt/SiO_2, vapor phase impregnation, DRIFTS, catalyst deactivation, diffusional effects on selectivity*

---

*To whom correspondence should be addressed: e-mail: resasco@ou.edu

ABSTRACT

The aromatization of *n*-octane was investigated on a Pt/KL catalyst prepared by vapor phase impregnation (VPI), a preparation method that in previous studies was found to result in the highest Pt dispersion and maximum incorporation of Pt inside the channels of the zeolite compared to any other method. Although the aromatization of *n*-octane on Pt/KL has been previously investigated, those studies were conducted on non-optimized catalysts. Our results show that, even on the Pt/KL catalyst prepared by the VPI method that exhibited optimum performance for the *n*-hexane aromatization, the activity for *n*-octane aromatization at 500°C and 1 atm was low and it quickly dropped after a few hours on stream.

The product distribution obtained from the *n*-octane conversion showed benzene and toluene as the dominant aromatic compounds, with small quantities of ethylbenzene (EB) and *o*-xylene (OX), which are the expected products from the direct closure of the six-member ring. The analysis of the product evolution as a function of conversion indicated that the benzene and toluene are secondary products resulting from the hydrogenolysis of ethylbenzene and *o*-xylene. Diffusional effects play a significant role in determining this product distribution. Since ethylbenzene and *o*-xylene are produced inside the channels of the zeolite, they are hydrogenolysed before they can escape. By contrast, on the Pt/SiO_2 catalyst used for comparison, ethylbenzene and *o*-xylene were the dominant aromatic products, although the overall aromatization activity was much lower than on the Pt/KL catalyst. The rapid deactivation found in the aromatization of *n*-octane on Pt/KL compared to that of *n*-hexane can also be explained in terms of the diffusional effects. The C8-aromatics produced inside the zeolite diffuse out of the system with much greater difficulty than benzene. Therefore, they form coke and plug the pores to a greater extent than benzene. Temperature programmed oxidation and sorption studies on spent samples demonstrate that the degree of pore blocking is much higher during *n*-octane aromatization than during *n*-hexane aromatization.

INTRODUCTION

The aromatization of *n*-alkanes is an important reaction with many industrial applications which could be carried out on both bifunctional (acid-metal) and monofunctional (only-metal) catalysts. The use of metal catalysts on non-acidic supports for this reaction have been a matter of research for many years. In 1969, Davis and Venuto [1] investigated the production of aromatic from different C8-C9 paraffin carbon skeleton structures over nonacidic Pt-Al_2O_3-K catalysts. In all cases, the aromatic products obtained were those predicted by a direct six-membered ring closure. Later, Davis *et al.* [2] further studied the addition of Sn to Pt / K-Al_2O_3. They found that the main C8 aromatic products were ethylbenzene and *o*-xylene and they were produced at a ratio near one, but on the catalyst containing Sn, the *o*-xylene production was favored. They also observed the same product distribution as the pressure was varied from 1 to 13 atm. In another study Davis *et al.* [3] observed that the Pt loading also influenced the distribution of aromatic products. From these two studies they concluded that these difference would suggest that the aromatization is a structure sensitive reaction, but found hard to explain how changes in structure can affect the ethylbenzene-to-*o*-xylene (EB/OX) ratio.

More closely related to the subject of the present work, Meriaudeau *et al.* [4] compared the aromatization of *n*-octane on Pt/SiO_2 and Pt/silicalite in order to study the role of support microporosity on the aromatic selectivity. With data from a pulse reactor, they demonstrated that the reaction over Pt/silicalite was strongly influenced by diffusional limitations, which lowered the overall conversion, but enhanced the selectivity towards ethylbenzene over other C8 aromatics.

The exceptionally high activity of Pt supported on alkaline L zeolites for the aromatization of *n*-hexane has been known for twenty years [5, 6]. The reaction mechanism for *n*-hexane aromatization on Pt/KL [7, 8] and the improvement of catalytic properties by varying promoters and preparation methods [9-16] have been the focus of many publications. Less attention has been dedicated to the

aromatization of longer chain alkanes, e.g. *n*-octane, on Pt/KL catalysts. One of the most complete studies of *n*-octane aromatization on Pt/KL was conducted by Huang *et al.* [12]. From their Carbon-14 tracer studies, they concluded that the behavior of the Pt/KL catalyst was very similar to that of other catalysts on non-acidic supports without microporosity. The unique behavior exhibited for *n*-hexane in terms of selectivity and catalyst life was not present for *n*-octane. However, the particular catalyst used in that study was prepared by the ion-exchange method and it is now known that this form of Pt incorporation results in a large fraction of metal clusters outside the channels of the zeolite [9]. During the last few years, we have studied methods of characterizing and maximizing the fraction of Pt clusters inside the L zeolite by incorporating the Pt via vapor-phase impregnation [11, 13-16]. Therefore, in this contribution, we report a study of the aromatization of *n*-octane as compared to *n*-hexane over a Pt/KL catalyst prepared by vapor-phase impregnation to determine whether a well-prepared Pt/KL catalyst can keep the excellent behavior observed for *n*-hexane aromatization.

EXPERIMENTAL

Catalyst Preparation: Pt/KL catalysts were prepared with 1 wt. % Pt by two methods; incipient wetness (IWI) and vapor phase impregnation (VPI), whereas Pt/SiO_2 catalyst was only prepared by the IWI method. The K-LTL-zeolite (Lot#1041, BET area = 292 m^2/g, SiO_2/Al_2O_3 ratio = 6) was produced by Tosoh Co. The precipitated silica Hi-Sil® 233 (CAS# 7631-86-9, BET area =140 m^2/g) was provided by PPG Siam Silica Co., Ltd. Prior to addition of the platinum metal, the supports were dried in an oven at 110°C overnight and calcined at 400°C in a dry air flow of 100 $cm^3/min.g$ for 5 h.

In the IWI method, tetraamineplatinum (II) nitrate (Merck) was weighed and dissolved in deionized water (0.69 cm^3/g support) and then impregnated over the dry support by slowly dropping the solution under a dry-nitrogen atmosphere. Next, the mixture was dried in an oven at 110°C overnight. The cool mixture was loaded into a glass tube and calcined at 350°C in a flow of dry air of 100 $cm^3/min.g$ for 2 h and

left to cool to room temperature. The resultant catalyst (Pt/KL-IWI or Pt/SiO_2) was stored in a desiccator. The Pt/KL-VPI catalyst was prepared by physically mixing weighed platinum (II) acetylacetonate (Alfa Aesar) and dry support under nitrogen atmosphere. The mixture was then loaded into the reactor tube under a He flow of 2 cm^3/min. The mixture was slowly ramped to 40°C and held there for 3 h, and ramped again to 60°C and held again for 1 h. After that, further ramped to 100°C, at which temperature the mixture was held for 1 h to sublime the $Pt(AcAc)_2$. After sublimation, the mixture was ramped to 130°C and held for 15 min to ensure that the entire precursor was sublimed. The reactor was cooled to room temperature. After that, it was ramped to 350°C in flow of air for 2 h and calcined at that temperature to decompose the Pt precursor. Finally, the Pt/KL prepared by the VPI method was stored in a desiccator.

Catalytic Activity Measurement: The catalytic activity studies were conducted at atmospheric pressure in a 0.5-inch glass tube with an internal K-type thermocouple for temperature measurement. The reactor was a single-pass, continuous-flow type, with a catalyst bed of 0.20 g. Prior to reaction, the temperature was slowly ramped in flowing H_2 at 100 cm^3/min.g for 2 h up to 500°C and in situ reduced at that temperature for 1 h. *n*-Hexane was added by injection from a syringe pump. In all experiments, the hydrogen to *n*-hexane (or *n*-octane) molar ratios was kept at 6:1. The products were analyzed in a Shimadzu GC-17A equipped with a capillary HP-PLOT/Al_2O_3 "S" deactivated column, using a temperature program to obtain optimal product separation. To identify m- and p-xylene, the analysis of the liquid product was performed in a capillary column AT™-1000. The activity data are reported in terms of total *n*-hexane or *n*-octane conversion and product selectivity, which is defined as weight of each individual product per weight of *n*-hexane or *n*-octane converted.

Hydrogen Chemisorption: The amount of adsorbed hydrogen on all fresh catalysts was measured in a static volumetric adsorption Pyrex system, equipped with a high capacity, high vacuum pump that provided vacuum on the order of 10^{-9} torr. Prior to

each experiment, 0.4 g of dried fresh catalyst was reduced in situ at 500°C for 1 h under flowing H_2, cooled down to 300°C, evacuated to at least 10^{-7} torr at 300°C for 20 min, then cooled down to room temperature under vacuum. Adsorption isotherms were obtained with several adsorption points ranging from 0 to 100 torr. The H/Pt values were directly obtained by extrapolating to zero pressure.

Diffuse Reflectance Infrared Fourier Transform Spectroscopy (DRIFTS) of Adsorbed CO: The fresh and spent Pt/KL and Pt/SiO_2 catalysts were characterized by DRIFTS using adsorbed CO as a probe in a Bio-Rad FTS-40 spectrometer equipped with a MCT detector. Experiments were performed in a diffuse reflectance cell from Harrick Scientific, type HVC-DR2, with ZnSe windows. For each IR spectrum, 128 scans were taken at a resolution of 8 cm^{-1}. Prior to taking each spectrum, a background was collected on the sample reduced in situ under a flow of H_2 at 300°C for 1 h and purged in He for 30 min at room temperature. Then, a flow of 3%CO in He for 30 min was sent over the sample, followed by a purge in He flow for 30 min. After this treatment, the spectrum of adsorbed CO was collected.

Temperature Programmed Oxidation (TPO): Temperature programmed oxidation was employed to analyze the amount and characteristics of the coke deposits on spent catalysts. TPO of the spent catalysts was performed in a continuous flow of 5% O_2/He while the temperature was linearly increased at a heating rate of 12°C/min. Before conducting the TPO on a 0.03 g sample placed in a ¼" quartz fixed-bed reactor, the spent catalyst was dried at 110°C overnight and weighed. The catalyst was then flushed by 5% O_2 in He for 30 min before the temperature ramp was started. The CO_2 produced by the oxidation of coke species was monitored by a mass spectrometer. The amount of coke was calibrated by using 100 µl pulses of pure CO_2. The evolved CO_2 partial pressure was normalized by the total pressure and the maximum signal in the pulses of CO_2.

iso-Butane Sorption: To determine the degree of pore plugging after reaction, the amount of iso-butane sorbed by the zeolite was measured on spent catalysts and

compared to that sorbed by the bare KL zeolite. The experiment was conducted in a volumetric system equipped with 0-100 torr MKS Barotron precision gauge. Prior to each adsorption run, the sample was activated by heating in vacuum (10^{-6} torr) at 350°C for 2 h; then, the temperature of the adsorbent bed was set to 100°C. The Pyrex system was also kept constant at 100°C by a heating tape connected to a temperature controller. A fixed amount of iso-butane (37 cm^3 at 100 torr and 100°C) was expanded into the adsorption cell (total volume = 54 cm^3). The total amount of isobutane sorbed was calculated from the pressure change.

RESULTS

Characterization of the Fresh Catalysts: The state of the fresh catalysts was characterized by H_2 and CO chemisorption after reduction in H_2 at 500°C. As shown in Table 1, the hydrogen uptake (H/Pt) values obtained on the Pt/KL-VPI, Pt/KL-IWI, and Pt/SiO_2 catalysts were 0.9, 0.6, and 0.2, respectively. These results are consistent with our previous work [14]. That is, the VPI catalyst exhibited higher H_2 uptake than the IWI catalyst. More important, the DRIFTS measurements of adsorbed CO showed that the VPI Pt/KL catalyst had the majority of the Pt clusters inside the channels of the zeolite. The CO spectra for the three catalysts investigated are shown in Fig. 1. In comparison with the Pt/SiO_2 catalyst, which displays a well-defined sharp peak at around 2074 cm^{-1} for the stretching frequency of linearly adsorbed CO, Pt/KL catalysts display complex bands which extend from 2080 cm^{-1} to much lower wavenumbers (e.g., as low as 1930 cm^{-1}). In a previous paper [14], we utilized DRIFTS of adsorbed CO to compare the morphology of Pt particles inside the KL zeolite, prepared by IWI and VPI methods. In that case, our results agreed very well with the hypothesis that CO itself modifies the structure of the small Pt clusters inside the KL zeolite. That is, CO adsorption does not probe the small metal particles in their original structure, but rather generates by disruption over time new molecular arrangements that are stabilized inside the zeolite [17]. In the presence of CO, Pt carbonyls can be formed and stabilized by the zeolite, which could act as a ligand. Previously published EXAFS data have shown that small Pt clusters present in the KL zeolite before the admission of CO can be completely

disrupted and new Pt-CO species are formed upon exposure to CO [18]. The important point to notice is that the formation of Pt carbonyls only occurs when the Pt clusters are very small. One may not expect the Pt particles outside the zeolite to be converted to Pt carbonyls. Therefore, FTIR of adsorbed CO is a useful technique for making general conclusions about the location (i.e., inside the L-zeolite or external) and distribution of the Pt clusters prior to disruption. For our purposes, the results strongly support the idea that the low wavenumber bands (below 2000 cm^{-1}) are related to the Pt clusters located inside the channels of the L-zeolite while the bands at and above 2075 cm^{-1} are due to the Pt external to the pores. In agreement with this assignment we saw, in our previous work, an increase in the intensity of the latter bands after agglomeration of the Pt clusters caused by oxidation-reduction cycles [11]. Finally, the bands between 2050-2000 cm^{-1} were assigned to CO adsorbed on particles near the pore mouth, although still inside the zeolite channels. By applying this analysis to the spectra of Fig. 1, one infers that the two Pt/KL catalysts have most of Pt particles inside the channel. As we have discussed previously [15], the H/Pt values are consistently lower for the IWI than for the VPI catalysts, which implies that, although in both cases the Pt is inside the zeolite channels, the metal clusters are smaller in the VPI catalysts. As previously shown, this smaller size imparts higher thermal stability to the clusters due to a more efficient interaction with the walls of the zeolite.

TABLE 1
Analysis data of fresh and spent Pt/KL catalysts

Catalyst	%Pt	H/Pt	Coke after C6 rxn (wt. %)	Coke after C8 rxn (wt. %)	i-C4 adsorbed on catalyst after C6 rxn*	i-C4 adsorbed on catalyst after C8 rxn*
Pt/SiO_2	1	0.2	-	-	-	-
Pt/KL-VPI	1	0.9	0.8	2.3	70	35
Pt/KL-IWI	1	0.6	1.5	2.1	-	-

* The data are in unit of percentage related to i-C4 adsorbed on bare KL zeolite.

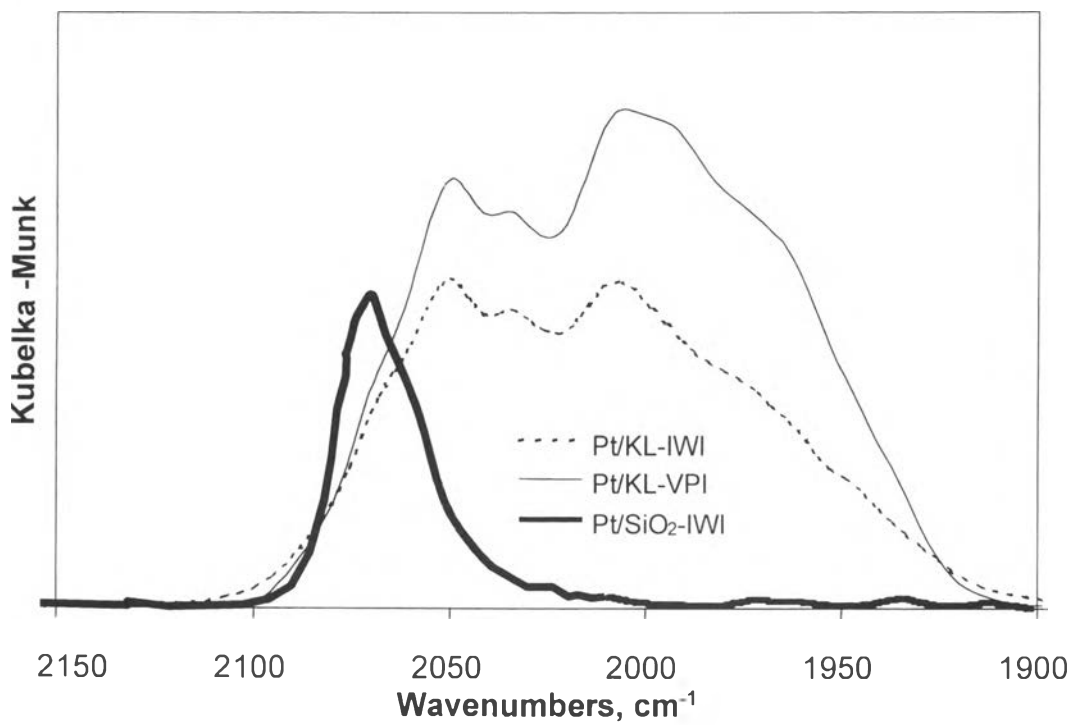

Fig. 1. DRIFTS spectra of CO adsorbed on Pt/KL-VPI, Pt/KL-IWI, and Pt/SiO_2 catalysts reduced in situ at 500°C. The reduced catalysts were exposed to a flow of 3%CO in He for 30 min at room temperature and purged in He for 30 min.

Catalytic Activity Measurements: The Pt/KL-VPI, Pt/KL-IWI, and Pt/SiO_2 catalysts were tested for the aromatization of *n*-octane and compared to that of *n*-hexane. The evolution of the conversion and total aromatics selectivity are shown in Fig. 2a and

b, respectively. In agreement with previous reports [13-15], the VPI Pt/KL exhibited the highest *n*-hexane aromatization conversion, benzene selectivity, and stability. Contrasting with the excellent performance obtained on this catalyst with *n*-hexane, the selectivity and stability were disapointingly low when the feed was changed to *n*-octane. In fact, Fig. 2a shows that for the *n*-octane aromatization the stability of Pt/SiO_2 was somewhat better than that of Pt/KL, although the overall conversion was very low. Interestingly, over the Pt/SiO_2 catalyst, the aromatic selectivity with *n*-octane was considerably higher than that with *n*-hexane, which contrasts with the behavior observed over the Pt/KL catalysts.

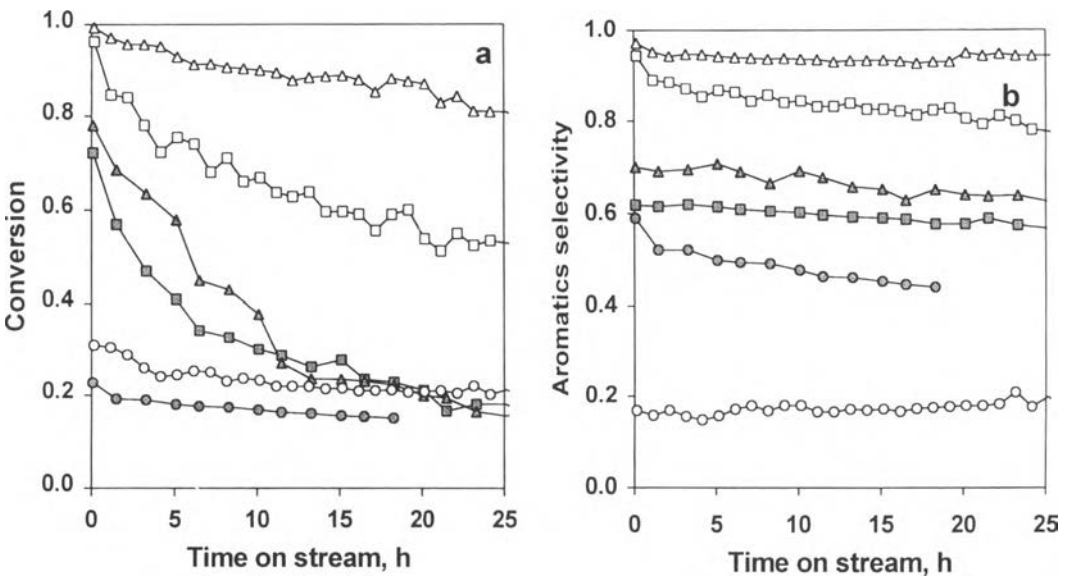

Fig. 2. (a) Total conversion of *n*-hexane (open symbols) and *n*-octane (full symbols) as a function of time on stream (b) Selectivity to total aromatics as a function of time on stream. Catalysts: Pt/KL-VPI (triangles), Pt/KL-IWI (squares), and Pt/SiO_2 (circles). Reaction conditions: 500°C, H_2/*n*-C6 (*n*-C8) molar ratio 6:1, WHSV 5 h^{-1}.

Table 2 summarizes the product distribution obtained after 10 h on stream over the Pt/SiO_2, Pt/KL-IWI, and Pt/KL-VPI catalysts for *n*-hexane and *n*-octane aromatization. As mentioned above, when *n*-hexane was the feed, the Pt/KL catalysts, particularly the one prepared by VPI, exhibited high conversion and high benzene selectivity while the Pt/SiO_2 showed much lower ability to produce aromatics. In fact, its main product was hexene from direct dehydrogenation. A

different result was obtained when *n*-octane was used as feed. Although the selectivity to total aromatics was higher over Pt/KL than on Pt/SiO_2, the aromatics obtained with Pt/KL were mostly benzene and toluene. By contrast, the Pt/SiO_2 catalyst produced mostly ethylbenzene (EB) and *o*-xylene (OX) as its dominant aromatization products, but no benzene was produced at any time. The differences in the aromatic product distribution obtained over Pt/KL and Pt/SiO_2 are better illustrated in Fig. 3, which shows the ratio of benzene to C8-aromatics produced from *n*-octane as a function of time on stream. This ratio was initially very high for the two Pt/KL catalysts. Although it decreased with time on stream, the amount of benzene was at any time higher than 3 times that of the *n*-octane aromatics.

TABLE 2

Product distribution of *n*-hexane and *n*-octane aromatization over different catalysts. Reaction conditions: 500°C, H_2/*n*-C6 (or *n*-C8) molar ratio 6:1,WHSV 5 h^{-1}

	Feed: *n*-hexane			**Feed: *n*-octane**		
	Pt/SiO_2	Pt/KL-IWI	Pt/KL-VPI	Pt/SiO_2	Pt/KL-IWI	Pt/KL-VPI
Conversion, % (after 10 h on stream)	18.8	71.1	90.6	16.8	30.1	37.7
Products selectivity, %						
C1-C5	8.8	22.4	12.2	7.1	34.0	29.4
Hexenes	78.7	5.9	0.7	3.5	1.2	0.7
Total aromatics	**15.1**	**85.6**	**93.6**	**48.8**	**60.2**	**69.2**
Benzene	15.1	85.6	93.6	0.0	27.4	27.7
Toluene	-	-	-	0.9	22.8	28.3
Heptenes	-	-	-	34.8	2.6	3.0
Octenes	-	-	-	5.4	1.4	1.9
Ethylbenzene	-	-	-	21.5	5.9	6.5
m-Xylene	-	-	-	1.2	1.1	1.2
p-Xylene	-	-	-	0.4	0.3	0.2
o-Xylene	-	-	-	24.8	2.8	3.0

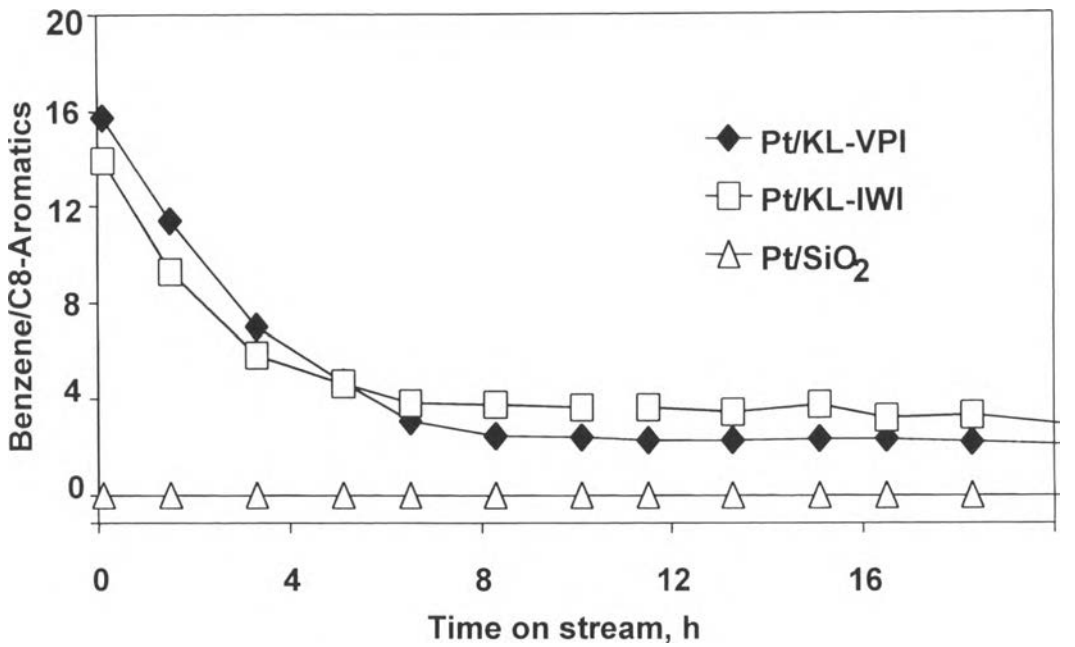

Fig. 3. Benzene to C8-aromatics product ratio during *n*-octane aromatization as a function of time on stream over Pt/KL-VPI, Pt/KL-IWI, and Pt/SiO_2 catalysts. Reaction conditions: 500°C, H_2/*n*-C8 molar ratio 6:1, WHSV 5 h^{-1}.

Another important difference between Pt/KL and Pt/SiO_2 is interesting to note. As shown in Table 2, over Pt/SiO_2 the production of OX was only slightly higher than that of EB. The decay of both products as a function of time was almost parallel. As a result, the EB/OX ratio remained constant with time on stream. On the other hand, Pt/KL exhibited a much higher production of EB than OX. The drop in OX production was much more rapid than that of EB. As illustrated in Fig. 4 the EB/OX product ratio obtained on the VPI Pt/KL catalyst rapidly increased during the first 7 h and stayed at a value of about 2.5, much higher than that reported for other Pt catalysts supported on non-acidic materials without micro-porosity [19]. A slight but clear difference between the IWI and VPI Pt/KL catalysts can be noted here. On the IWI catalyst, the EB/OX ratio started at a high value of about 2.0 from the very first moments on stream. After about 7 h, this ratio was about the same for both catalysts. As discussed below, it is important to note that high EB/OX ratios have only been observed on Pt/zeolite catalysts [4], which reveals the role that shape-selectivity may have in this reaction. Therefore, the difference observed on the two Pt/KL catalysts

before coke deposition might be related to slight differences in the molecular transit inside the zeolite pores related to the different metal particle sizes. After several hours on stream, the coke deposits that partially block the pores may erase the initial differences.

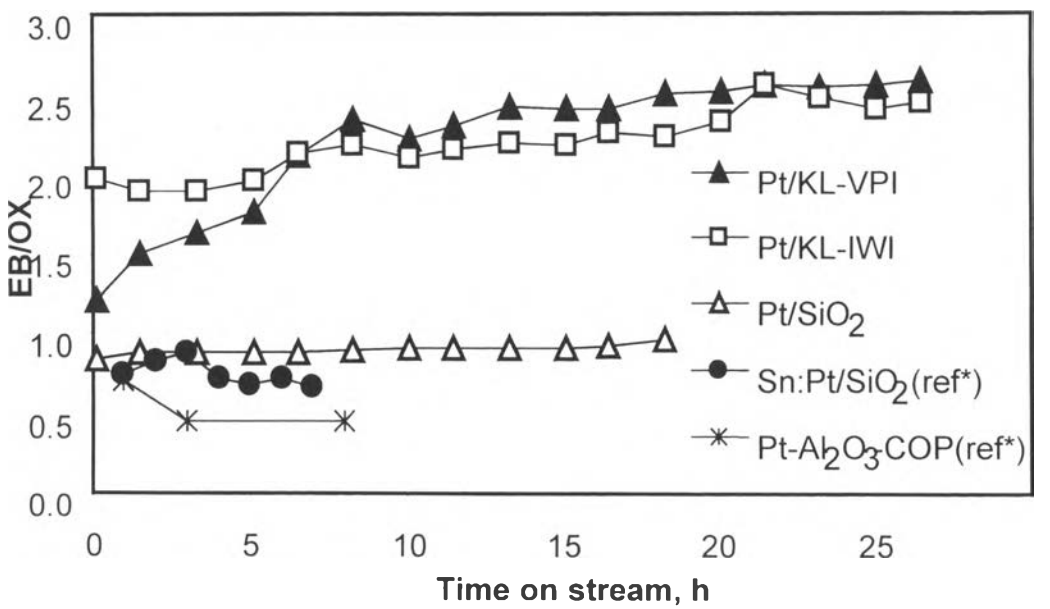

Fig. 4. Ethylbenzene:*o*-xylene (EB/OX) ratio during *n*-octane aromatization over Pt/KL-VPI, Pt/KL-IWI, and Pt/SiO_2 catalysts. Reaction conditions: 500°C, H_2/*n*-C6 (*n*-C8) molar ratio 6:1,WHSV 5 h^{-1}. Included for comparison are data adapted from ref. [2].

Figure 5a shows the variation of the steady-state product selectivity with conversion as the reaction temperature was varied from 300 to 500 °C, at a fixed WHSV=5 h^{-1}. It can be observed that the selectivity to methane continuously increased with conversion. The selectivity to C8-aromatics exhibited a maximum at about 6.5% conversion and then it decreased. This decrease is accompanied by an increase in the production of benzene, indicating that benzene is a secondary product, which results from hydrogenolysis of C8-aromatics, rather than from cyclization of previously hydrogenolysed *n*-octane. The detailed product distribution and the corresponding temperatures and conversions are shown in Table 3, which clearly illustrates the enhanced hydrogenolysis of EB and OX to benzene and toluene at higher temperatures. Figure 5b shows a similar graph of steady-state selectivity vs.

conversion, but in this case, the conversion was varied by changing the WHSV from 9 to 1 h^{-1}, at a fixed temperature (500°C). In line with the results obtained by varying the temperature, the data shows that at higher conversions the selectivity to C8-aromatics dropped while the amount of benzene and methane increased. The detailed product distribution is reported in Table 4. An interesting trend in the EB/OX ratio as a function of space velocity is clearly apparent. As illustrated in Fig. 6, the EB/OX ratio markedly drops approaching a value of about one as the space velocity decreases.

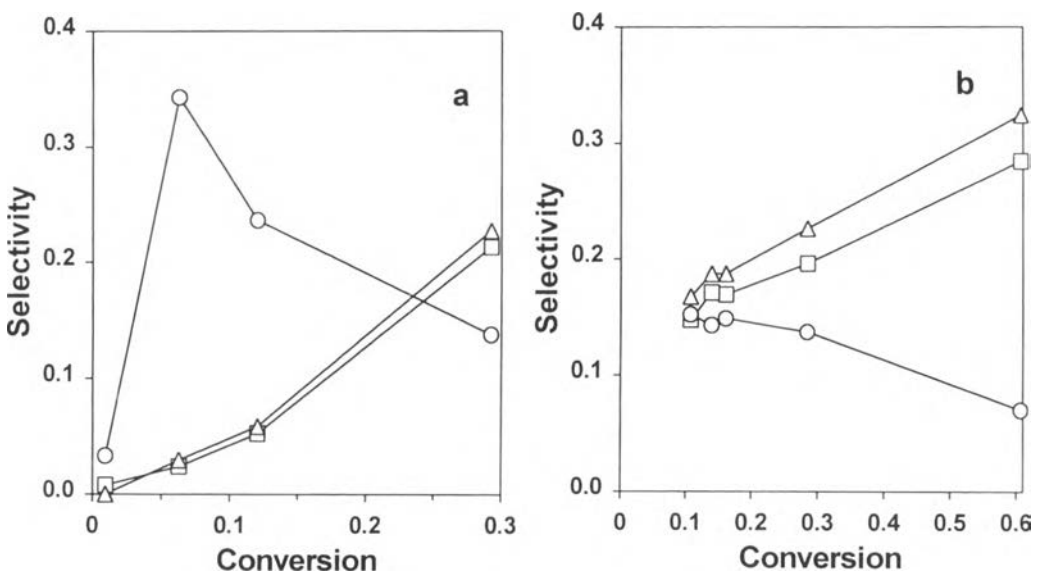

Fig. 5. Steady-state product selectivity as a function of conversion during *n*-octane aromatization. (a) Conversion varied by increasing temperature from 300 to 500 °C, at a fixed WHSV=5 h^{-1}. (b) Conversion varied by changing the WHSV from 9 to 1 h^{-1}, at a fixed temperature, 500°C. circles: C8-aromatics; triangles: toluene; squares: methane.

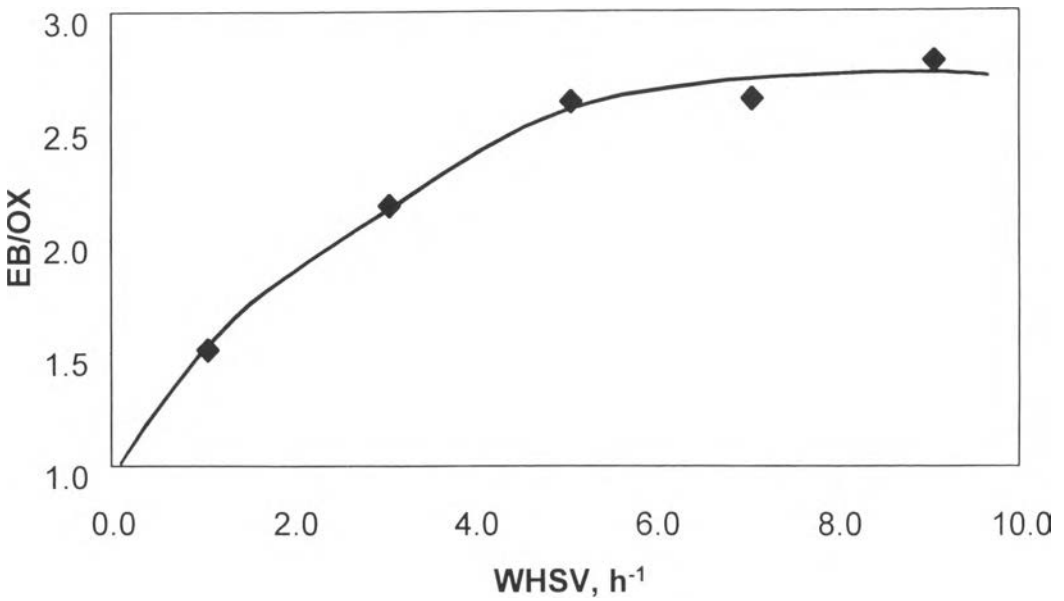

Fig. 6. Ethylbenzene:*o*-xylene (EB/OX) ratio during *n*-octane aromatization over the Pt/KL-VPI catalyst as a function of space velocity. Reaction conditions: 500°C, H_2/*n*-C6 (*n*-C8) molar ratio 6:1, 10 h on stream.

TABLE 3

Product distribution of *n*-octane aromatization over Pt/KL-VPI at various reaction temperatures. Reaction conditions: H_2/*n*-C8 molar ratio 6:1,WHSV 5 h^{-1}

	Reaction Temperature, °C				
	300	**350**	**400**	**450**	**500**
Conversion, %	0.2	1.0	6.3	12.1	29.3
Products selectivity, %					
C1-C5	1.4	1.4	4.2	9.4	28.9
Hexenes	3.9	16.8	7.0	5.5	1.5
Benzene	0.0	0.0	3.0	5.9	22.7
Toluene	0.0	18.2	19.0	24.0	25.5
Heptenes	66.6	45.2	24.9	22.4	4.5
Octenes	28.1	15.2	7.6	9.2	3.1
Ethylbenzene	0.0	0.0	20.6	15.7	8.6
m- and *p*-Xylenes	0.0	3.3	2.8	1.9	1.4
o-Xylene	0.0	0.0	11.0	6.1	3.8

TABLE 4

Product distribution of *n*-octane aromatization over Pt/KL-VPI at various WHSV. Reaction conditions: 500°C, H_2/*n*-C8 molar ratio 6:1

	WHSV, h^{-1}				
	1.0	**3.0**	**5.0**	**7.0**	**9.0**
Conversion, %	60.7	28.5	16.1	14.0	10.7
Products selectivity, %					
C1-C5	34.5	28.5	26.4	26.7	24.1
Hexenes	0.65	1.9	2.7	2.8	3.1
Benzene	32.5	22.6	18.7	18.7	16.7
Toluene	23.3	26.1	25.1	24.8	25.1
Heptenes	1.0	3.1	4.6	4.3	5.1
Octenes	1.0	4.0	7.4	8.2	10.4
Ethylbenzene	3.5	8.2	9.6	9.2	10.0
m- and *p*-Xylenes	1.1	1.6	1.6	1.6	1.6
o-Xylene	2.4	3.9	3.7	3.5	3.6

TABLE 5

Product distribution of different feeds over Pt/KL-VPI catalysts.

Reaction conditions: 500°C, H_2/reactant molar ratio 6:1,WHSV 5 h^{-1}

	Reactant				
	***n*-Octane**	**Ethylbenzene**	***o*-Xylene**	**Toluene**	***n*-Heptane**
Conversion, %	37.7	71.5	16.7	64.9	36.4
Products selectivity, %					
C1-C2	27.0	20.1	11.8	15.4	21.6
C3-C5	2.4	0.0	0.0	0.0	6.2
Hexenes	0.7	0.00	0.0	0.0	7.5
Benzene	27.7	46.5	6.4	84.3	28.5
Toluene	28.3	32.9	78.9	-	33.1
Heptenes	3.0	0.0	0.0	0.0	2.3
Octenes	1.9	0.0	0.2	0.0	0.0
Ethylbenzene	6.5	-	0.2	0.0	0.0
m- and *p*-Xylenes	1.4	0.0	1.8	0.0	0.0
o-Xylene	3.0	0.2	-	0.0	0.0

Another important aspect observed in the product distributions obtained at various temperatures and space velocities is the absence of products that could be associated with a C5-ring closure. For example, methylcyclopentane, 2- or 3- methylpentane were only present at the level of traces in the product from the *n*-hexane reaction. Similarly, negligible amounts of iso-octanes, methylcyclopentane, or other alkylcyclopentanes were obtained from the *n*-octane reaction.

To further investigate the effect of secondary reactions on the product distribution, we conducted activity measurements using *n*-C7 as well as C7 and C8 aromatics as feed, keeping the same H_2:reactant molar ratio of 6:1 as for the *n*-octane activity measurements. The results obtained at 500°C and at a WHSV of 5 h^{-1} are summarized in Table 5. The vast majority of the products of C8 aromatics come from hydrogenolysis of the alkyl groups attached to the aromatic ring. The

conversion of EB and OX only resulted in C1, C2, benzene, and toluene. No ring opening products and very small amount of isomerization products were observed. Very different deactivation patterns were exhibited by the different aromatic compounds. As illustrated in Fig. 7, the OX conversion dropped much more rapidly than the EB conversion, which could be explained in terms of the different diffusion rates of the two aromatics through the zeolite channels. To illustrate this difference, the interaction of EB, OX, and toluene with the KL zeolite was further investigated using the static volumetric adsorption apparatus. The uptakes of EB, OX, and toluene after exposing the bare zeolite to the same initial pressure of hydrocarbon vapor are summarized in Table 6. It is seen that the OX uptake was significantly lower than those of EB and toluene, which can be rationalized in terms of the critical molecular diameters relative to the zeolite pore size. The pore size of the KL zeolite is 0.71 nm [20], which is larger than critical diameters of EB and toluene but smaller than that of OX. Therefore, one can expect that the mobility of OX inside the channels of the zeolite will be very much restrained.

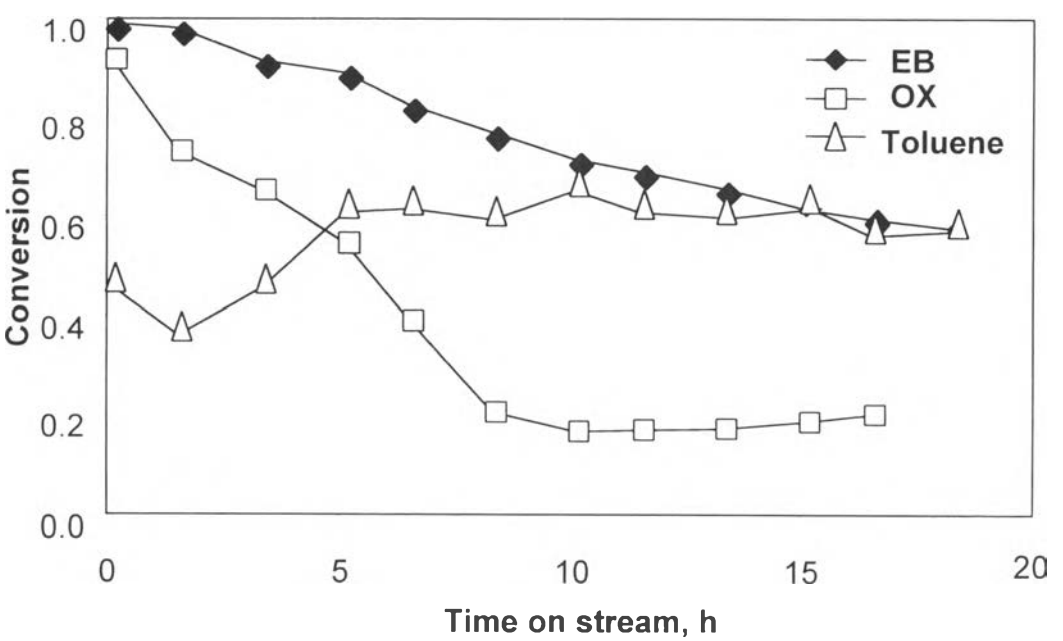

Fig. 7. Total conversion of different hydrocarbons over the Pt/KL-VPI catalyst as a function of time on stream. Reaction conditions: 500°C, H_2/hydrocarbon molar ratio 6:1,WHSV 5 h^{-1}.

TABLE 6

Diffusibility of different aromatics into channel of L zeolite

	Toluene	**Ethylbenzene**	**Ortho-xylene**
Temperature (°C)	180	180	180
Initial Moles in Cell	7.6×10^{-5}	7.1×10^{-5}	6.9×10^{-5}
Equilibrium Pressure (Torr)	1.7	2.5	5.9
Moles Adsorbed	5.7×10^{-5}	4.4×10^{-5}	0.6×10^{-5}
Critical Molecular Diameter (nm)	0.67	0.67	0.74

Characterization of the Spent Catalysts: The coke residues left on the catalyst during reaction were quantified by TPO. Table 1 summarizes the amounts of coke deposited during 9 h on stream with *n*-hexane and *n*-octane reactions on the different catalysts. On the VPI Pt/KL catalyst, more than twice as much coke was deposited during the *n*-octane aromatization as during *n*-hexane aromatization, which parallels the faster rate of deactivation observed with *n*-octane. The corresponding TPO profiles are shown in Figure 8. Not only the overall oxygen consumption, but the relative size of the peaks are clearly different. The large oxidation peak appearing at high temperature after *n*-octane reaction is possible due to the plugging of zeolite pores, which would retard the oxidation of the coke deposits. On the IWI catalyst, the difference between the amount of coke deposited with *n*-octane and with C6 was not as great, but it must be noted that the IWI catalyst already had twice as much coke as the VPI catalyst after the *n*-hexane reaction.

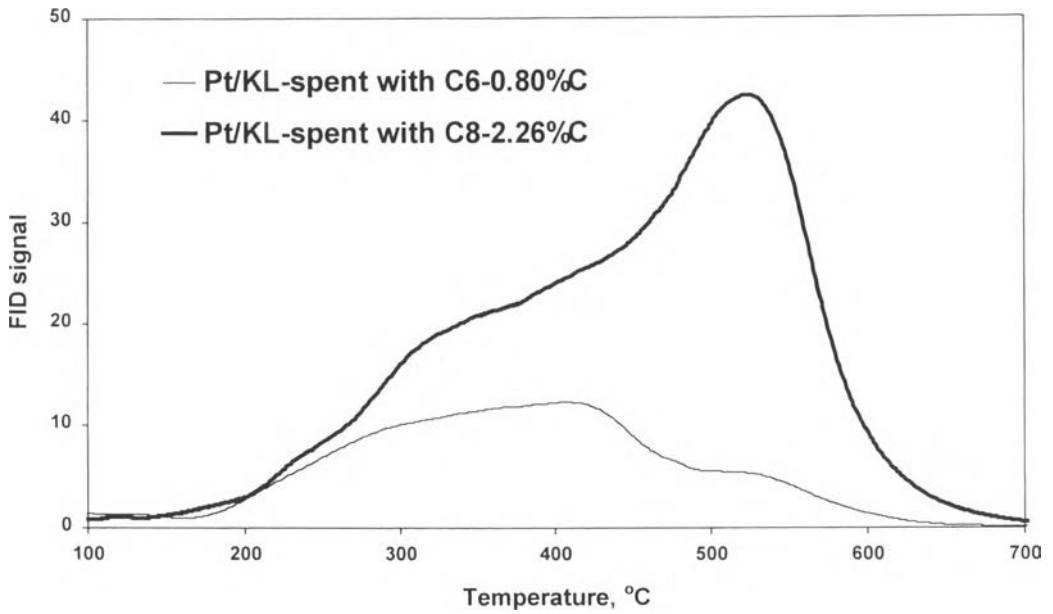

Fig. 8. Temperature programmed oxidation (TPO) profiles of coke deposits left over the Pt/KL-VPI catalyst after 9 h on stream during *n*-hexane (thin line) and *n*-octane aromatization (heavier line). Reaction conditions: 500°C, H_2/*n*-C6 (or *n*-C8) molar ratio 6:1,WHSV 5 h^{-1}.

To confirm that pore blocking of L-zeolite is more pronounced under *n*-octane reaction than under *n*-hexane reaction, sorption of a small molecule like isobutane was used as a probe of the zeolite pore volume accessible after reaction. Table 1 shows the sorption capacity values obtained on the VPI Pt/KL catalyst after 9 h reaction periods at 500°C and at a WHSV of 5 h^{-1}, using *n*-octane and *n*-hexane feeds. The two values are reported relative to the isobutane sorption capacity of the bare zeolite. It can be observed that while after reaction with *n*-hexane, 70% of the zeolite pores were available, only 35 % remained were available after the *n*-octane reaction.

***Regeneration of Spent Catalysts*:** To investigate whether the fast deactivation observed under C8 aromatization can be reversed by oxidizing the coke deposits, we have conducted two consecutive reaction cycles with an intermediate regeneration step consisting in oxidizing the carbon deposits in air flow for 90 min at 400°C, followed by reduction at 500°C for 60 min. Before the oxidation step, the *n*-octane

flow was stopped and the catalyst left at 500°C under hydrogen flow for 60 min. The amount of coke present after each of these cycles was quantified by TPO. It was observed that after the regeneration procedure, the amount of carbon left on the catalyst was about one third of that present after the reaction cycle. Interestingly, even though a significant fraction of carbon remained on the catalyst after this treatment, the initial activity and selectivity was regained. The evolution of conversion and selectivity during the initial and second cycles is illustrated in Fig. 9. It is clear that not only the initial activity was regained after regeneration, but also the deactivation pattern was almost identical to that of the fresh catalyst. There was a small variation in the evolution of EB/OX ratio as a function of time on stream. The EB/OX ratio on the second cycle seems to increase a little faster than on the fresh catalyst. This slight difference could be due to a higher inhibition of the OX mobility inside the channels of the zeolite caused by the presence of the fraction of carbon residues not removed by the regeneration or to a small metal particle growth. Still, this difference is very small compared to that observed in Fig. 4 with the IWI catalyst.

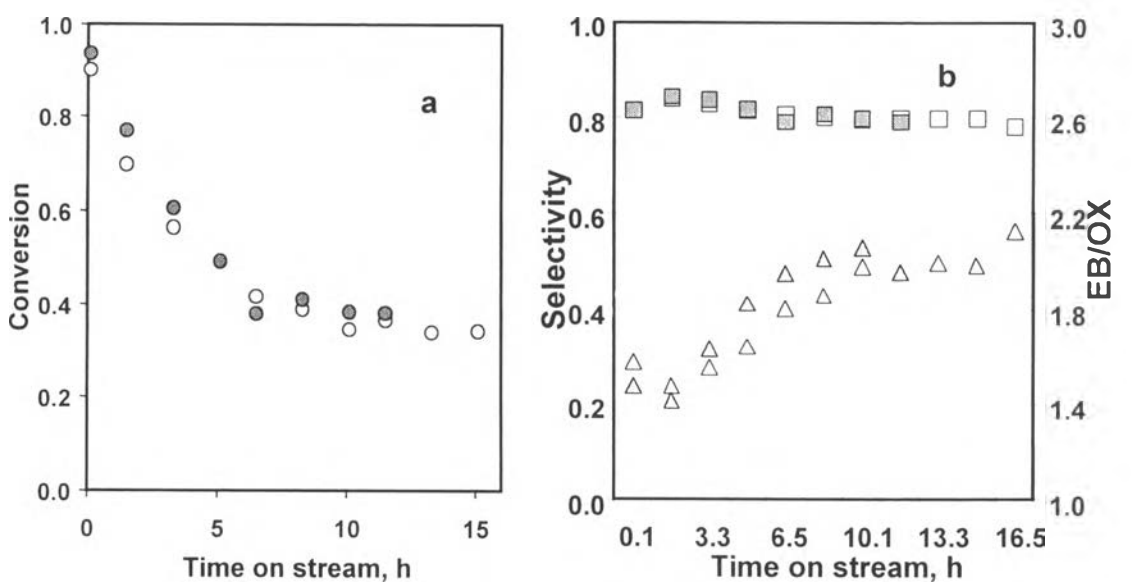

Fig. 9. (a) Total *n*-octane conversion before and after regeneration in air at 400°C as a function of time on stream. Open symbols: first reaction cycle; full symbols: reaction cycle after regeneration. (b) Left axis: Selectivity to total aromatics; Right axis: Ethylbenzene:*o*-xylene (EB/OX) ratio.

DISCUSSION

In contrast to the results obtained by Huang *et al.* [12] on a Pt/KL catalyst prepared by ion exchange, the differences observed in this work between Pt/KL and Pt/SiO_2 are significant. The product distribution clearly indicates that the effect of the zeolite structure plays a major role in determining selectivity. By comparing the data on the two Pt/KL catalysts one can see that although the differences between the behavior of the VPI and IWI catalysts is not so pronounced with *n*-octane as with *n*-hexane, there are still some advantages on the VPI catalyst related to its more homogenous distribution of small Pt clusters inside the zeolite. Both, the overall conversion and the selectivity to total aromatics are higher. Nonetheless, the catalytic performance displayed by even our best Pt/KL formulation (VPI) is unsatisfactory for the aromatization of *n*-octane under the conditions of this study (500°C, 1 atm). Contrary to the high stability displayed by the VPI Pt/KL in the aromatization of *n*-hexane, severe deactivation is observed with *n*-octane. The conversion dropped drastically during the first 10 h on stream while the selectivity to aromatics was much lower than that obtained with *n*-hexane. The TPO and iso-butane adsorption results indicate that the activity drop must be due to the blockage of zeolite pores by the coke deposits.

On the Pt/SiO_2 catalyst, the conversion level did not differ much from *n*-hexane to *n*-octane. However, an important difference was observed in the selectivity to aromatics, which was much higher for *n*-octane than for *n*-hexane. This difference might be due to the known increase in ring closure activity as the chain length increases [21].

Interesting observations have been made in the product distribution obtained on the different catalysts. Over Pt/SiO_2, the main aromatic products from *n*-octane were EB and OX which are the only two expected products from direct six membered ring closure [1, 2, 22]. Although on the Pt/KL catalysts the dominant C8-aromatics were also EB and OX, the majority of the aromatic products obtained were benzene and toluene, which result from secondary reaction of EB and OX. It is interesting to

compare the relative amount of EB and OX that do not undergo secondary hydrogenolysis by measuring the EB/OX ratio in the products. On the Pt/SiO_2 catalyst, this ratio was almost one, which is the same as that observed in previous studies using non-acidic non-zeolitic supports (e.g. SiO_2 [12]and $K\text{-}Al_2O_3$ [2, 19]). The ratio did not change much as a function of time on stream. By contrast, on the Pt/KL it changed both as a function of time and as a function of space velocity. At very low space velocities it was also near one, but as the space velocity increased, the EB/OX ratio greatly increased. Similarly, the ratio greatly increased as a function of time on stream. These selectivity changes can all be explained in terms of diffusional effects in and out of the zeolite.

A few years ago, Meriaudeau *et al.* [4] observed high EB/OX ratios over Pt/silicalite. They proposed that the diffusion of products affects the rate of reaction and product selectivity and ascribed the higher conversion of *n*-C8 to EB compared to that to OX to a faster diffusion rate of EB through the zeolite channels. They indicated that the fact that a difference in conversion was observed demonstrated that the mass transfer was the rate limiting step. Our results suggest that although differences in diffusion rates may affect the product distribution, the observed differences in conversion do not necessarily imply that mass transfer is rate limiting. We have previously observed important shape-selective effects in the hydrogenolysis of methylcyclopentane, that were easily explained in terms of restriction in the passage of hydrocarbons through the channels of the KL zeolite. In that case, the preferred orientation of the MCP molecule along the molecular axis resulted in enhanced production of 3MP relative to 2MP [23]. Here, we can expect that the EB molecule can diffuse more rapidly through the KL zeolite channels than OX. This restrictive movement results in a longer residence time of OX than EB inside the zeolite channel. Therefore, one does not need to invoke that diffusion is the rate limiting step to explain the change in the EB/OX ratio. When the OX and EB are produced inside the zeolite, the OX is more effectively converted into benzene and toluene than the EB. Therefore, even though the six-member ring closure may not favor EB over OX, the resulting EB/OX ratio is larger than that originally produced. This analysis gives further support to the above conjecture that the Pt/KL catalyst

employed in ref. [12], which was prepared by the ion-exchange method, had the majority of the Pt outside the channels of the zeolite [9, 15] and so it behaved like Pt/SiO_2. In that case, the EB/OX ratio was near one because there was very little effect of the zeolite structure.

In the experiments conducted at low space velocities one may expect that EB would have the time to come out of the zeolite and reenter, so eventually the secondary conversion erases the differences as it is experimentally verified (see Fig. 6). As the space velocity increases, the EB that diffuses out of the zeolite is removed more quickly from the catalyst bed and does not have time to continue reacting.
The more rapid deactivation displayed when the reactant was OX than when it was EB (see Fig. 7) also reflects the longer residence time that the OX molecule may have inside the zeolite. Another evidence for the important role of diffusion in selectivity is the variation of the EB/OX ratio as a function of time on stream. As shown in Fig. 4, the ratio on the very clean VPI Pt/KL catalyst is initially near unity, but very rapidly starts increasing as coke begins to make the diffusion of OX through the pores more difficult. On the IWI catalyst, the presence of larger Pt clusters makes the diffusion of OX slower, even on the clean catalyst. As a result, the EB/OX ratio on this catalyst is higher from the start.

It is highly possible that the C8 aromatics produced inside the channels of the zeolite are responsible for the rapid deactivation observed during *n*-octane aromatization, as oppossed to the high stability displayed during *n*-hexane aromatization. As mentioned above, they may spend more time inside the zeolite and they are the only new species that appear in the system, compared to the situation in *n*-hexane aromatization. The other species that could result in coke formation are benzene and olefins, but they are also present during the *n*-hexane aromatization, but they cause no significant deactivation when the Pt/KL catalyst is well prepared.

The final observation that is worth mentioning is that the product distribution obtained from *n*-octane aromatization indicates that the formation of five-member ring intermediates is very low. Only traces of branched alkanes and essentially no

alkyl-cyclopentanes were observed at any conversion. It has been shown that during *n*-hexane aromatization, five-member ring closure occurs to a much lower extent than six-member ring closure [24]. The same difference seems to be present during *n*-octane aromatization.

CONCLUSIONS

Pt/KL catalysts are not as effective for the aromatization of *n*-octane as they are for the aromatization of *n*-hexane. Even on a well-prepared Pt/KL catalyst that exhibits excellent performance under *n*-hexane, the deactivation is rapid under *n*-octane and the selectivity to C8 aromatics is low. This low selectivity is due to secondary hydrogenolysis of C8 aromatics to benzene and toluene. The hydrogenolysis of the C8 aromatics is particularly pronounced with *o*-xylene, which diffuses through the zeolite channels much less rapidly than benzene, toluene, or even ethylbenzene, that is the other C8 aromatic produced from direct ring closure.

ACKNOWLEDGEMENTS

This work was supported by The Thailand Research Fund under the Royal Golden Jubilee Ph.D. program and basic research project. Part of the experimental work was supported by the Oklahoma Center for the Advancement of Science and Technology (OCAST).

REFERENCES

1. Davis, B. H. and Venuto, P. B., *J. Catal.* **15** 363 (1969).
2. Davis, B. H., *J. Catal.* **42** 376 (1976).
3 Davis, B. H., Westfall, G. A., and Naylor, R. W., *J. Catal* **42** 238 (1976).
4. Meriaudeau, P., Thangaraj, A., Naccache, C., and Narayanan, S., *J. Catal.* **146** 579 (1994).
5. Bernard, J. R., Proc. 5th Internat. Zeolite Confer., (L. V. C. Rees, editor) Heyden, London 686 (1980).
6. Davis R. J., *in* "HCR Concise Review", J. Wiley, N. York 41 (1994).

7. Derouane, E. G. and Vanderveken, D. J., *Appl. Catal.* **45** L15 (1988).
8. Tauster, S. J. and Steger, J. J., *J. Catal.* **125** 387 (1990).
9. Ostgard, D. J., Kustov, L., Poeppelmeier, K. R., and Sachtler, W. M. H., *J. Catal.* **133** 342 (1992).
10. Li, F. X., Zhou, Q., and Luo, L., *Appl. Catal.* **161** 227 (1997).
11. Jacobs, G., Ghadiali, F. , Pisanu, A., Padro, C. L., Borgna, A., Alvarez, W. E., and Resasco, D. E., *J. Catal.* **191** 116 (2000).
12. Huang, C-S, Sparks, D. E., Dabbagh, H. A., and Davis, B. H., *J. Catal.* **134** 269 (1992).
13. Jacobs, G., Padro, C. L., and Resasco, D. E., *J. Catal.* **179** 43 (1998).
14. Jacobs, G., Ghadiali, F. , Pisanu, A., Borgna, A., Alvarez, W. E., and Resasco, D. E., *Appl. Catal.* **188** 79 (1999).
15. Jacobs, G., Alvarez, W. E., and Resasco, D. E., *Appl. Catal.* **206** 267 (2001).
16. Ghadiali, F., Jacobs, G., Pisanu, A., Borgna, A., Alvarez, W. E., and Resasco, D. E., *Stud. Surf. Sci. Catal.* A. **130** 2537 (2000).
17. Stakheev, A. Y., Shpiro, E.S., Jaeger, N.I., and Schulz-Ekloff, G., *Catal. Lett.* **34** 293 (1995).
18. Mojet, B.L., Miller, J.T., and Koningsberger, D.C., *J. Phys. Chem. B* **103** 2724 (1999).
19. Srinivasan, R. and Davis, B. H., *J. Mol. Catal.* **88** 343 (1994).
20. Barrer, R.M. and Villiger, H. Z., *Kristallogr.* **128** 352 (1969).
21. Somorjai, G. A., Proc. 8th Int. Congr. Catal., Verlag Chemie, Weinheim, Fed. Rep. Ger. 1, I113-I150 (1984).
22. Gault, F. G., *Adv. Catal.* **30** 1 (1981).
23. Alvarez, W. E. and Resasco, D. E., *Catal. Lett.* **8** 53 (1991).
24. Miller J. T., Agrawal, N. G. B., Lane, G. S., and Modica, F. S., *J. Catal.* **163** 106 (1996).